

# **Lawrence Berkeley National Laboratory**

## **LBL Publications**

### **Title**

Highly Efficient Ternary Solar Cells with Efficient Förster Resonance Energy Transfer for Simultaneously Enhanced Photovoltaic Parameters

### **Permalink**

<https://escholarship.org/uc/item/6f96x9mx>

### **Journal**

Advanced Functional Materials, 31(41)

### **ISSN**

1616-301X

### **Authors**

Xiao, Liangang

Wu, Xing

Ren, Guoxing

et al.

### **Publication Date**

2021-10-01

### **DOI**

10.1002/adfm.202105304

Peer reviewed

**Highly Efficient Ternary Solar Cells with Efficient Förster Resonance Energy Transfer for Simultaneously Enhanced Photovoltaic Parameters**

Liangang Xiao<sup>a</sup>, Xing Wu<sup>a</sup>, Guoxing Ren<sup>a</sup>, Matthew A. Kolaczkowski<sup>b</sup>, Guang Huang<sup>d</sup>, Wanyi Tan<sup>a</sup>, Lin Ma<sup>d</sup>, Yidong Liu<sup>a</sup>, Xiaobin Peng<sup>c</sup>, Yonggang Min<sup>\*a</sup> and Yi Liu<sup>\*b</sup>

Prof. L. G. Xiao, X. Wu, G. X. Ren, Prof. W. Y. Tan, Prof. Y. D. Liu, Prof. Y. G. Min  
School of Materials and Energy, Guangdong University of Technology, Guangzhou 510006, China

E-mail: ygmin@gdut.edu.cn

Dr. Matthew A. Kolaczkowski, Dr. Y. Liu

The Molecular Foundry, Lawrence Berkeley National Laboratory, Berkeley, CA, 94720, USA  
E-mail: [yliu@lbl.gov](mailto:yliu@lbl.gov)

Prof. X. B. Peng

State Key Laboratory of Luminescent Materials and Devices, Institute of Polymer Optoelectronic Materials and Devices, South China University of Technology, Guangzhou 510640, China

G. Huang, Prof. L. Ma

School of Physics and Optoelectronic Engineering, Guangdong University of Technology, Guangzhou 510006, China

Keywords: energy transfer, high open-circuit voltage, molecular mixture, non-fullerene acceptors, ternary solar cells

**Abstract**

Introducing a third component into organic bulk heterojunction solar cells has become an effective strategy to improve the photovoltaic performance. Meanwhile, the rapid development of non-fullerene acceptors (NFAs) has pushed the power conversion efficiency (PCE) of organic solar cells (OSCs) to a higher standard. Herein, a series of fullerene-free ternary solar cells have been fabricated based on a wide bandgap acceptor, IDTT-M, together with a wide bandgap donor polymer PM6 and a narrow bandgap NFA Y6. Insights from the morphological and electronic characterizations reveal that IDTT-M has been incorporated into Y6 domains without disrupting its molecular packing and sacrificing its electron mobility, and work synergistically with Y6 to regulate the packing pattern of PM6, leading to enhanced hole mobility and suppressed recombination. IDTT-M further functions as an energy-level mediator that increases open-circuit voltage ( $V_{OC}$ ) in ternary devices. In addition, efficient

Förster resonance energy transfer (FRET) between IDTT-M and Y6 provides a non-radiative pathway for facilitating exciton dissociation and charge collection. As a result, the optimized ternary device features a significantly improved PCE up to 16.63% with simultaneously enhanced short-circuit current ( $J_{SC}$ ),  $V_{OC}$  and fill factor (FF).

## 1. Introduction

Organic solar cells (OSCs) are promising for the next-generation photovoltaic technology which feature low cost fabrication and flexibility and are also compatible with high throughput large-scale production.<sup>[1]</sup> In the past two decades, benefiting from the development of electron donor materials, the power conversion efficiency (PCE) of solar cells devices has been significantly enhanced. Many prominent donor materials such as PTB7-Th, PffBT4T and BTID-2F, when combined with PC<sub>71</sub>BM, delivered a high PCE more than 10%.<sup>[2]</sup> However, the absorption bands of the blend of these donor materials with fullerene-based acceptors can not match the whole solar spectrum, leading to limited photocurrent and a significant waste of solar energy. The inadequate absorption range and inefficient power conversion are the main culprits for the plateau in PCE enhancement. Therefore, it is essential to further improve the performance via device fabrication engineering, such as tandem and multicomponent solar cells.<sup>[3]</sup> However, it is hard for tandem solar cell to realize large-scale and high-throughput production due to its complex fabrication processes. Introducing additional components to fabricate ternary solar cells poses a much smaller barrier to adoption by maintaining a simple device fabrication process. The simplicity and high performance of ternary cells paves an effective way to obtain highly efficient solar cells devices.<sup>[4]</sup> For example, highly efficient ternary solar cells could be fabricated based on two narrow bandgap non-fullerene acceptors (NFAs) with similar chemical structures, delivering enhanced hole transfer and decreased energy loss.<sup>[4i, 4j]</sup> Adding a third component with reduced miscibility

and complementary absorption to the host materials enables ternary solar cells with improved short-circuit current ( $J_{SC}$ ) and fill factor (FF).<sup>[4k, 4l]</sup> In addition, PC<sub>71</sub>BM has been employed in ternary solar cells to tune light absorption and phase segregation along vertical direction of the active layer.<sup>[4m, 4n]</sup>

Thanks to the rapid development of NFAs, remarkable progress has been made to accelerate the field of organic photovoltaics into a new phase, in which the PCE of the devices has already soared to over 16%,<sup>[5]</sup> and thermal and light stabilities have also been significantly improved. Y6 and ITIC are two representative narrow band-gap NFAs, both of which are acceptor-donor-acceptor (A-D-A) type structures, leading to efficient intra-molecular charge transfer and red-shifted absorption.<sup>[6]</sup> So far, Y6 and its derivatives, when combined with the wide band-gap donors, deliver the highest efficiency solar cells devices. For example, Li et al. fabricated polymer solar cells based on PTQ10 and Y6, and the devices exhibited a high PCE of 16.53% with  $J_{SC}$  of 26.65 mA cm<sup>-2</sup> and open-circuit voltage ( $V_{OC}$ ) of 0.826 V.<sup>[7]</sup> Zou et al. reported a series of Y6 derivatives with different alkyl chain and fabricated efficient solar cells with the largest PCE of 15.98% using a wide bandgap donor PM6 and chloroform solvent.<sup>[8]</sup> However, these devices always feature the characteristics of high  $J_{SC}$  but moderate  $V_{OC}$  due to the low lowest unoccupied molecular orbital (LUMO) energy level of the NFAs. Generally, the electron withdrawing ability of the end-capped groups allows the LUMO energy level to be raised or lowered and slightly affects the highest occupied molecular orbital (HOMO) energy level. Weakly electron withdrawing end groups are suitable for raising the LUMO energy level in such NFAs, which are responsible for higher  $V_{OC}$  and potentially enhanced PCE in the corresponding devices.<sup>[9]</sup> The research efforts on wide bandgap acceptors have demonstrated success in the fabrication of high  $V_{OC}$  solar cells, the overall device performance are however suboptimal with unsatisfying short-circuit currents ( $J_{SCs}$ ).<sup>[10]</sup> One of the few strategies for addressing the trade-off between  $V_{OC}$  and  $J_{SC}$  has been to employ wide bandgap

acceptors in organic solar cells which are capable of efficient Förster resonance energy transfer (FRET) between the different components in ternary solar cells. This FRET enhancement has been quite effective in improving the  $J_{SC}$  at little expense of  $V_{OC}$ .<sup>[11]</sup>

Recently, we reported a series of high LUMO energy level NFAs bearing different alkyl chains on the weakly electron-withdrawing thiobarbituric acid end groups and revealed the ideal window of crystallinity associated with the hydrocarbon chains.<sup>[12]</sup> Solar cells based on the NFA with shorter methyl group (IDTT-M) showed a high  $V_{OC}$  of 1 V when paired with the PTB7-Th polymer donor. As IDTT-M has exhibited high crystallinity with large crystal correlation length and good film morphology when spin coated from chloroform, it is employed as a third component to the well-studied PM6:Y6 system for fabricating ternary solar cells, in anticipation that its strong crystallinity could modulate molecular packing in ternary blend films for efficient charge transportation. In this contribution, binary solar cells based on PM6 and IDTT-M was fabricated to deliver an optimal PCE of 7.78% with a  $J_{SC}$  of 11.05 mA cm<sup>-2</sup> and a high  $V_{OC}$  of 1.16 V. In comparison, we fabricated a series of ternary solar cells with different weight ratios of IDTT-M. At the optimal weight ratio of 15 wt%, the corresponding best device delivered a highest PCE of 16.63% with simultaneously enhanced  $J_{SC}$ ,  $V_{OC}$  and FF compared to the corresponding PM6:Y6 binary device. A systematic study of the ternary device characteristics revealed that efficient FRET has taken place between IDTT-M and Y6 without disrupting the bi-continuous PM6:Y6 blend film morphology, which provided a non-radiative path for IDTT-M in ternary system and also an additional pathway to promote exciton separation. Improved hole transfer and hole mobility, as well as enhanced charge separation and collection with suppressed charge recombination were all observed, contributing to the elevated FF and  $J_{SC}$ . Additionally, the  $V_{OC}$  of the ternary device was increased due to the higher LUMO energy level of IDTT-M compared to that of Y6. All these features contribute synergistically towards an improved PCE in ternary solar cells. This work

elucidates the significant role of wide bandgap NFAs in improving performance of ternary organic solar cells and further promoting the development of photovoltaic technology.

## 2. Results and Discussions

Ternary solar cells were fabricated with a conventional configuration (**Figure 1a**) and chemical structures of PM6, Y6 and IDTT-M were shown in **Figure 1b**. The normalized absorption properties of neat films were displayed in **Figure 1c**. The absorption band of PM6 is mainly located in the wavelength range from 500 to 650 nm with two peaks at 572 and 613 nm. Y6 exhibits a broad absorption band to the near infrared region with a maximum absorption peak at 816 nm. For IDTT-M, the absorption spectrum mainly falls in the range of 550 to 700 nm with the highest extinction coefficient larger than  $1.6 \times 10^5 \text{ cm}^{-1}$  (**Figure S1**). **Figure S2** shows the absorption spectra of ternary blend films with fixed electron donor/acceptor weight ratio but varying IDTT-M components. Increasing the weight ratio of IDTT-M obviously enhances the absorption intensity in the range of 530 to 650 nm, together with a slight decrease of the absorption intensity between 700 and 850 nm because of the diminished contribution from Y6

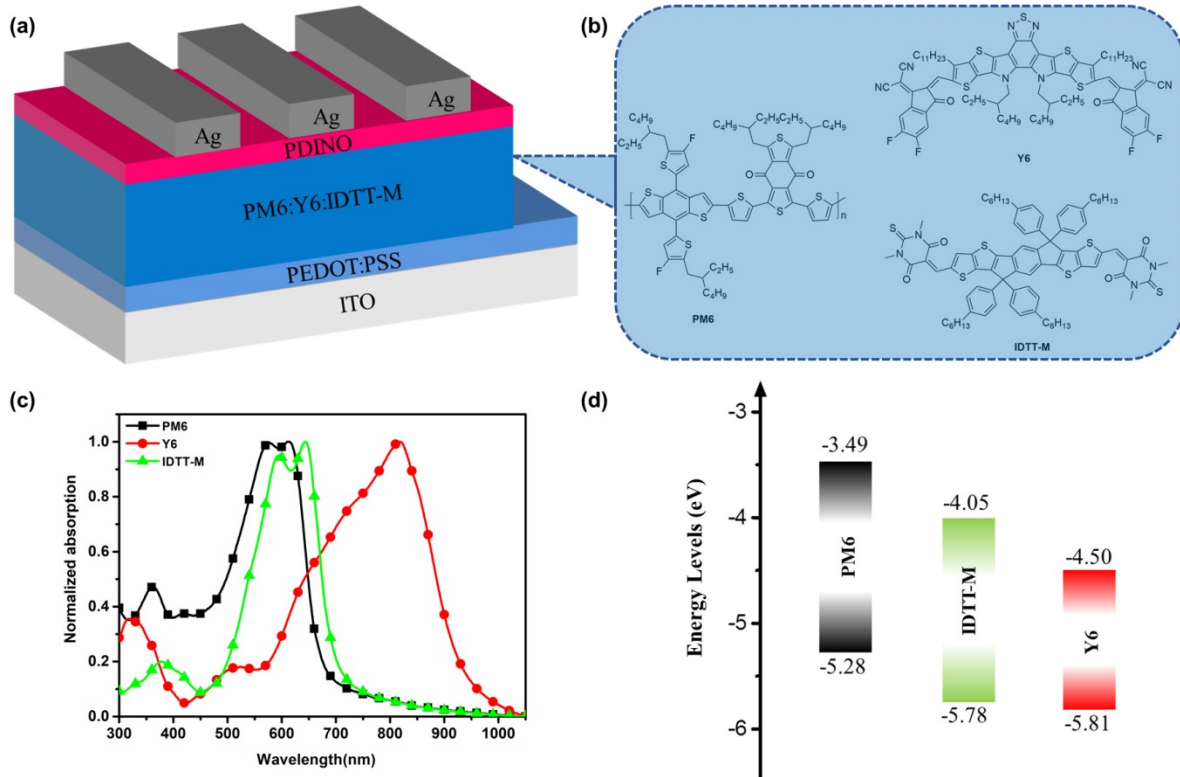


**Figure 1.** (a) Device configuration, and (b) chemical structures of PM6, Y6 and IDTT-M; (c) absorption spectra, and (d) energy levels of neat PM6, Y6 and IDTT-M films; the HOMO energy levels of these films were obtained by photoemission yield spectroscopy in air (PYSA) and the LUMO energy levels were calculated from HOMO energy levels and optical bandgaps.

**Table 1.** Photovoltaic performance of ternary solar cells devices with different weight ratios of IDTT-M.

PM6:Y6:IDTT-M	$J_{SC}$ (mA cm $^{-2}$ )	$V_{OC}$ (V)	$FF$ (%)	$PCE$ (%)
1:1.2:0	25.41 (24.97) <sup>a</sup>	0.841	72.45	15.48 <sup>b</sup> (15.32) <sup>c</sup>
1:1.08:0.12	25.60 (25.19) <sup>a</sup>	0.862	72.95	16.10 <sup>b</sup> (15.98) <sup>c</sup>
1:1.02:0.18	25.81 (25.31) <sup>a</sup>	0.872	73.89	16.63 <sup>b</sup> (16.45) <sup>c</sup>
1:0.96:0.24	24.88 (24.22) <sup>a</sup>	0.877	72.64	15.85 <sup>b</sup> (15.70) <sup>c</sup>
1:0.84:0.36	23.68(23.13) <sup>a</sup>	0.889	68.00	14.32 <sup>b</sup> (14.11) <sup>c</sup>
1:0:1.2	11.05 (10.68) <sup>a</sup>	1.16	60.70	7.78 <sup>b</sup> (7.70) <sup>c</sup>

a) values in parentheses are  $J_{SCS}$  calculated from EQE curve; b) the best PCE; c) values in parentheses are average PCEs from ten devices.

The photovoltaic parameters of binary and ternary solar cells based on different compositions of IDTT-M were investigated by fabricating the devices with a conventional structure of ITO/PEDOT:PSS/PM6:Y6:IDTT-M/PDINO/Ag. The overall donor and acceptor ratio was fixed at 1:1.2. The active layers were initially optimized from chloroform solution with a PM6 concentration of 5 mg mL<sup>-1</sup>. The current density versus voltage (*J*-*V*) curve is shown in **Figure 2a** and **Figure S3**, and corresponding photovoltaic parameters of devices with different weight ratio of Y6 under AM 1.5G spectrum from a solar simulator with the illumination at 100 mW/cm<sup>2</sup> were listed in **Table 1**. The optimal PM6:IDTT-M based binary solar cell exhibited a moderate PCE of 7.75% and a considerably lower *J<sub>SC</sub>* of 11.05 mA cm<sup>-2</sup> due to the limited absorption of the sunlight. However, IDTT-M showed a high-lying LUMO energy level of -3.72 eV, and thereby delivered a very high *V<sub>OC</sub>* of 1.16 V. The control binary device of PM6:Y6 displayed a *J<sub>SC</sub>* of 25.41 mA cm<sup>-2</sup>, a *V<sub>OC</sub>* of 0.841 V, an FF of 72.45% and a PCE of 15.48%. After adding IDTT-M into the PM6:Y6 blend, *J<sub>SC</sub>* and FF elevated initially and reach the maximum when the weight ratio of Y6:IDTT-M is 1.02:0.18, However, a further increase of IDTT-M composition led to the decrease of *J<sub>SC</sub>* and FF, and consequently low PCEs. The *V<sub>OC</sub>*, on the other hand, increased monotonically from 0.841 to 1.16 V with the increase of the weight ratio of IDTT-M from 0 wt% to 100 wt%. Compared to the control device, the optimized ternary devices achieved a higher *J<sub>SC</sub>* of 25.81 mA cm<sup>-2</sup> and FF of 73.89%, as well as an increased *V<sub>OC</sub>* of 0.872 V, leading to an improved PCE of 16.63%. Generally, *V<sub>OC</sub>* is determined by the acceptor with the lower LUMO level in ternary system with two electron acceptors.<sup>[13]</sup> The monotonic increase of *V<sub>OC</sub>* at increasing composition of IDTT-M indicated the formation of alloy-like electron acceptors from blending IDTT-M and Y6, which facilitated charge collection via separate charge-transfer paths from both IDTT-M and Y6 to the electrode.<sup>[14]</sup>

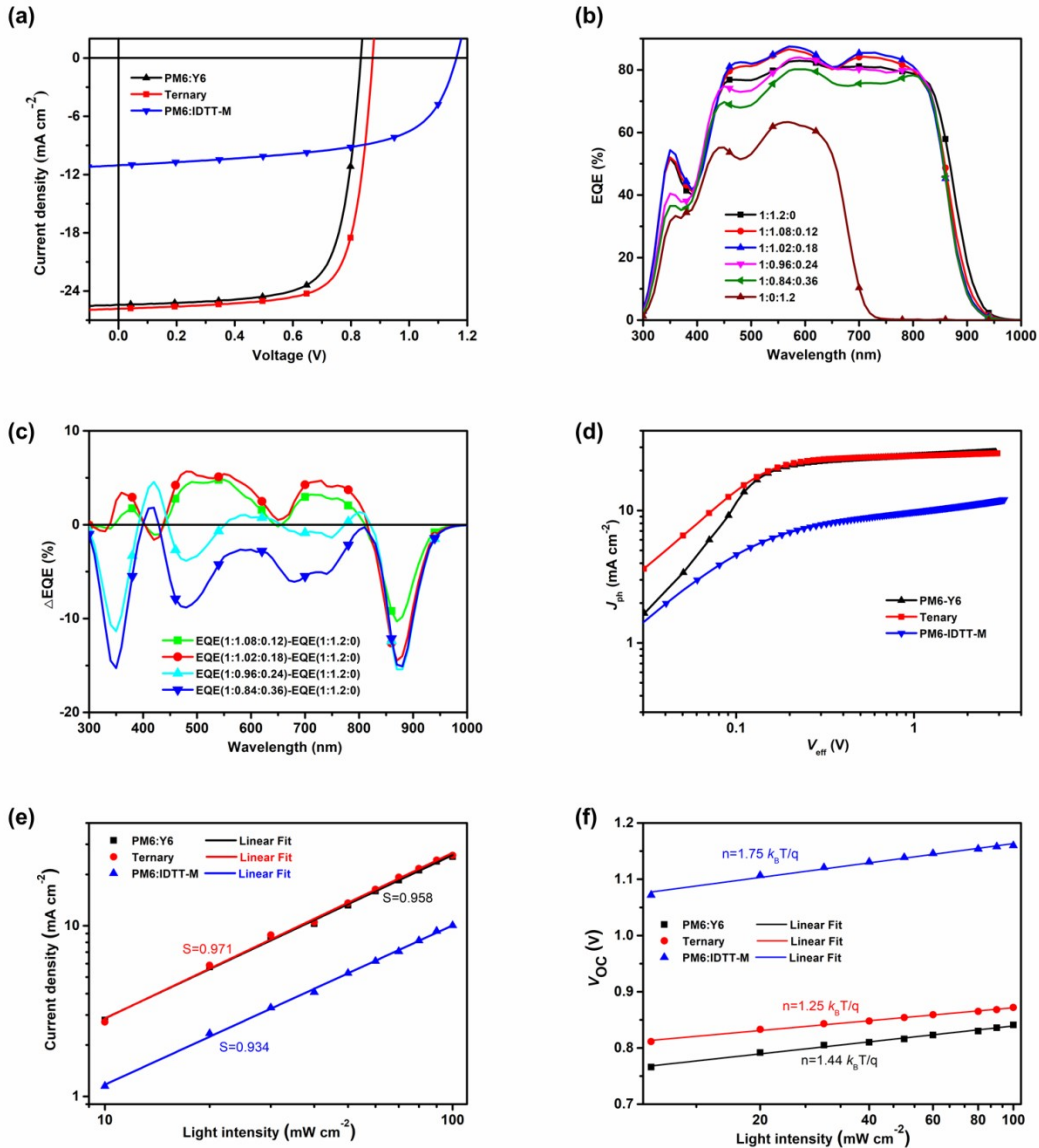


**Figure 2.** (a) Representative  $J$ - $V$  curves of the binary and ternary solar cells, (b) the EQE curves of solar cells, (c) the differences in EQE spectra and the legends indicating weight ratios of PM6:Y6:IDTT-M, (d) the  $J_{\text{ph}}$ - $V_{\text{eff}}$  curves of typical solar cells, (e) the dependence of  $J_{\text{SC}}$  on light intensity of typical solar cells, (f) the dependence of  $V_{\text{OC}}$  on light intensity of typical solar cells.

The external quantum efficiency (EQE) of binary and ternary OSCs with different weight ratio of IDTT-M was measured to investigate the photon-response of devices at different wavelength and crosscheck the reliability of the photocurrents from the  $J$ - $V$  measurements. As shown in **Figure 2b**, ternary and PM6:Y6 based binary devices show broad photon-responses

which are mainly located in the range of 400 to 900 nm, while the photon-response of PM6:IDTT-M based device just falls in a limited region between 400 and 700 nm, accompanied with notably lower EQE values. For easy comparison of the EQE changes, the difference EQE ( $\Delta$ EQE, defined by  $\text{EQE}_{\text{ternary}} - \text{EQE}_{\text{binary}}$ ) plots were illustrated in **Figure 2c**. Ternary device (PM6:Y6:IDTT-M=1:1.02:0.18) exhibits slightly lower EQE values in the range of 830 to 950 nm but enhanced EQE values in the range of 450 to 650 nm compared to the PM6:Y6 binary device, which agrees with the absorptivity of IDTT-M. Interestingly, simultaneous enhancement of EQE values of ternary device (IDTT-M<15 wt%) in the range of 700 to 830 nm are also observed in spite of the decreased absorptivity due to the decreased Y6 in the ternary blend. Higher loading of IDTT-M (IDTT-M>30 wt%) lead to significantly decreased EQE values in the whole region. The EQE enhancement and the absorptivity decrease in the range of 700 to 830 nm are inversely correlated, indicating that there is an additional photoelectric conversion process, instead of direct photo-excitation, to compensate for the decreased photocurrent caused by the decrease of direct light absorption to afford an overall enhanced  $J_{\text{SC}}$  in ternary devices. The integrated  $J_{\text{SC}}$  extracted from EQE values (**Table 1**) are consistent with the current densities from  $J$ - $V$  measurement.

To get deeper insights into the charge dynamics (exciton dissociation and charge transportation processes) of solar cells devices, the dependence of the photo-generated current density ( $J_{\text{ph}}$ ) on the effective voltage ( $V_{\text{eff}}$ ) of optimized ternary and corresponding binary devices were measured.<sup>[15]</sup> As shown in **Figure 2d**, for the PM6:Y6 and PM6:Y6:IDTT-M (1:1.02:0.18) based solar cell devices under high reverse bias voltage regime ( $V_{\text{eff}} > 2.0$  V),  $J_{\text{ph}}$  becomes saturated ( $J_{\text{sat}}$ ) which indicates that almost all excitons are dissociated into free charges and further collected by the corresponding electrodes. The ratios of  $J_{\text{ph}}/J_{\text{sat}}$  under short-circuit current condition were used to estimate the charge dissociation probabilities ( $P(E,T)$ ). The determined  $P(E,T)$  values were 95.0% and 97.2% for the PM6:Y6 and

PM6:Y6:IDTT-M (1:1.02:0.18) based devices, respectively. Charge collection efficiency calculated from  $J_{\text{ph}}/J_{\text{sat}}$  under maximum power output condition also showed similar improvement from 84.9% to 87.9%. Furthermore, the highest  $J_{\text{ph}}$  in the low  $V_{\text{eff}}$  region also indicated the excellent charge collection efficiency for the ternary device. The enhanced  $P(E,T)$  and charge collection efficiency suggested that incorporating 15 wt% IDTT-M could promote charge dynamics in ternary blend device. We also measured the  $J$ - $V$  characteristics under different light intensity and plotted the dependences of  $J_{\text{SC}}$  and  $V_{\text{OC}}$  on light intensity ( $P_{\text{light}}$ ) to investigate recombination processes in devices. According to the relationship of  $J_{\text{SC}} \propto (P_{\text{light}})^S$ , the power-law exponential factor  $S$  is effective to evaluate the degree of bimolecular recombination within the device.<sup>[16]</sup> For a device with negligible bimolecular recombination,  $S$  value would equal to 1. As shown in **Figure 2e**, the fitting  $S$  values are 0.958, 0.971, and 0.934 for the PM6:Y6, PM6:Y6:IDTT-M (1:1.02:0.18), and PM6:IDTT-M based devices. The  $S$  value for the PM6:Y6:IDTT-M (1:1.02:0.18) based device is much closer to 1, suggesting that the bimolecular recombination could be suppressed with the incorporation of 15 wt% IDTT-M. The degree of trap-assisted Shockley-Read-Hall or the geminate recombination could be investigated by applying the  $V_{\text{OC}}$  as a function of the natural logarithm of  $P_{\text{light}}$ , which is expressed as  $V_{\text{OC}} \propto n(K_B T/q) \ln(P_{\text{light}})$ , where  $K_B$  is the Boltzmann's constant,  $T$  is the Kelvin temperature in Kelvin,  $q$  is the elementary charge.<sup>[17]</sup> As shown in **Figure 2f**, the slope of PM6:IDTT-M based device is  $1.75 K_B T/q$ , indicating significant trap-assisted Shockley-Read-Hall or the geminate recombination. For the devices based on PM6:Y6 and the PM6:Y6:IDTT-M (1:1.02:0.18) based device, the slope is decreased from  $1.44 K_B T/q$  to  $1.25 K_B T/q$ . This tendency verifies that trap-assisted Shockley-Read-Hall or the geminate recombination was effectively suppressed. In

addition, we measured carrier mobility of devices by using space charge limited current method. As shown in **Figure S4** and **Figure S5**, the calculated results showed that the hole mobility were increased from  $5.23 \times 10^{-4} \text{ cm}^2 \text{ V}^{-1} \text{ s}^{-1}$  (PM6:Y6 based device) to  $6.44 \times 10^{-4} \text{ cm}^2 \text{ V}^{-1} \text{ s}^{-1}$  (PM6:Y6:IDTT-M (1:1.02:0.18) based device), while the electron mobility of both devices is about  $3.70 \times 10^{-4} \text{ cm}^2 \text{ V}^{-1} \text{ s}^{-1}$ , which shows negligible change (**Table S1**). Taken together, reduced bimolecular and monomolecular recombination and enhanced hole mobility are observed in the optimal ternary solar cell, which contribute to the enhanced  $J_{SC}$  and FF.

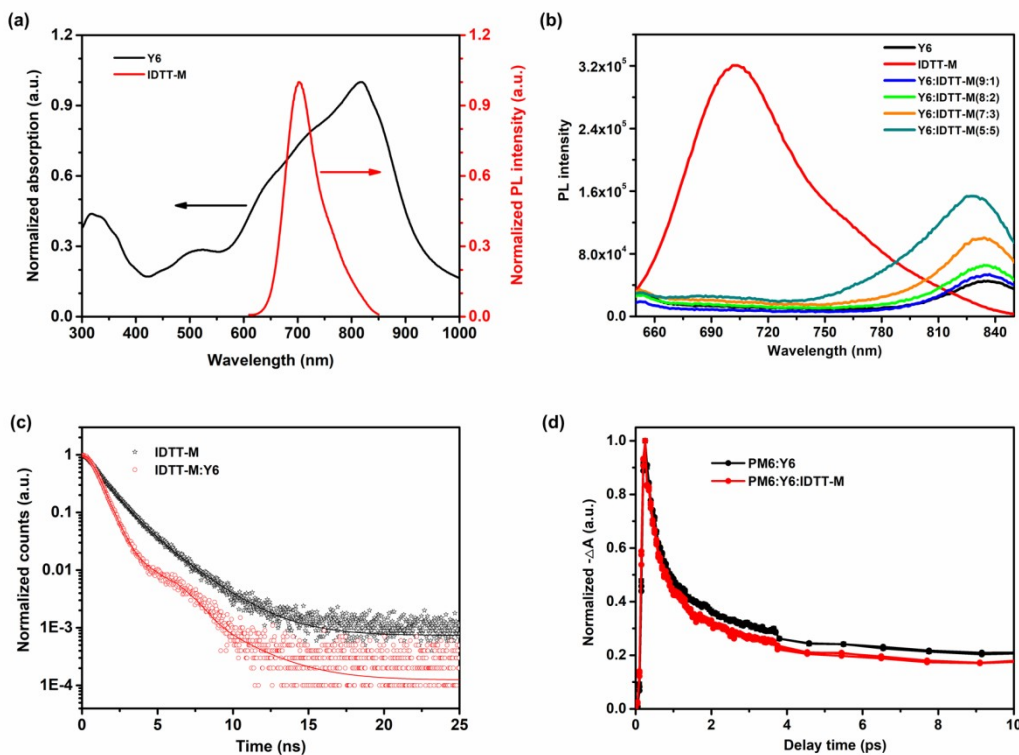


**Figure 3.** (a) Normalized absorption spectra of Y6 film and photoluminescence spectra of IDTT-M film; (b) PL spectra of Y6, IDTT-M, and their mixtures at the weight ratios of 9:1, 8:2, 7:3 and 5:5 (excitation wavelength of 594 nm); (c) Normalized time-resolved photoluminescence spectra of neat IDTT-M film and IDTT-M:Y6 blend film with a weight ratio of 1:1; (d) Transient absorption kinetics of PM6:Y6 and PM6:Y6:IDTT-M(1:1.02:0.18) blend films probed at 710 nm.

To understand the enhanced exciton dynamic processes in the multi-component systems, we measured steady-state photoluminescence (PL) spectra of films of individual components and those with various ratio of IDTT-M as the third component at excitation wavelength of 594 nm. The emission spectrum of IDTT-M and absorption spectrum of Y6 are shown in **Figure 3a**. An apparent overlap indicates the possibility of energy transfer between IDTT-M (FRET donor) and Y6 (FRET acceptor). As reported previously, non-radiative FRET results from long-range dipole-dipole interactions between FRET donor and acceptor pair, and has been demonstrated as an effective way to improve the performance of ternary solar cells.<sup>[18]</sup> We thus investigated the PL of IDTT-M:Y6 blend films as a function of the weight ratio (10 % to 50% IDTT-M). As displayed in **Figure 3b**, the emission at 703 nm corresponds to pure IDTT-M, and the maximum PL peak of pure Y6 was located at 833 nm. For the IDTT-M:Y6 blend films with different weight ratios, the PL emission at 703 nm was completely quenched and only one maximum PL peak at the position close to Y6 emission was observed. Furthermore, the PL emissions of blend films were monotonously enhanced with the increased weight ratio of IDTT-M from 10% to 50% in the blend films. The phenomenon observed in the steady-state PL measurement indicated efficient FRET between IDTT-M and Y6. In addition, we further conducted time-resolved photoluminescence (TRPL) spectra to confirm the FRET from IDTT-M to Y6. **Figure 3c** displays time correlated photon counting spectra of neat IDTT-M film and that of the blend film based on IDTT-M and Y6 at the weight ratio of 1:1. The average fluorescence lifetime was calculated to be 1.1 ns for IDTT-M and 0.6 ns for IDTT-M:Y6 blend film, respectively. Indeed, an additional decay channel in the blend film is present and the fluorescence lifetime of IDTT-M decreases (represented by an additional, faster time constant of 0.5 ns) upon adding Y6. Such a behavior is a solid evidence for efficient energy transfer from IDTT-M toward Y6. Considering that the donor-acceptor separation should be within 10 nm for efficient FRET, the observed energy transfer indicated

that IDTT-M and Y6 are well mixed and closely packed. Femtosecond transient absorption (TA) spectroscopy was employed to investigate the hole transfer dynamics in the multicomponent blend films following selective excitation of Y6 at 750 nm for monitoring the spectral dynamics of the entire system. **Figure S6** presents the two-dimensional TA color plots of a binary blend of PM6:Y6 and a ternary blend of PM6:Y6:IDTT-M in the range of 500 to 950 nm. Their correspondingly representative TA spectra at different delay times are depicted in **Figure S7**. As evident from TA spectra of neat Y6 film (**Figure S8**), the clear bleach characteristics at 780-840 nm in the PM6:Y6 binary film is mainly from the ground state bleaching (GSB) signatures of the Y6 acceptor. The negative signals appearing at the wavelength of 630 nm can be attributed to GSB response features of PM6, which suggests ultrafast hole transfer from Y6 to PM6. Except for the absorption intensity, there is no obvious spectral differences for the PM6:Y6 binary film and PM6:Y6:IDTT-M ternary film. The kinetic decay processes of PM6:Y6 and PM6:Y6:IDTT-M were further probed at 710 nm and illustrated in **Figure 3d**. For the sake of comparison, the data are normalized at the pump pulse peak. The relaxation rate becomes faster in the PM6:Y6:IDTT-M ternary blend than that of PM6:Y6 binary blend in a broad time scale. These differences convincingly revealed that there are more efficient channels for improved hole transfer when IDTT-M was added as the third component. The more efficient energy transfer and improved hole transfer correlate well with the enhanced quantum efficiency and charge dynamics in ternary blend devices.

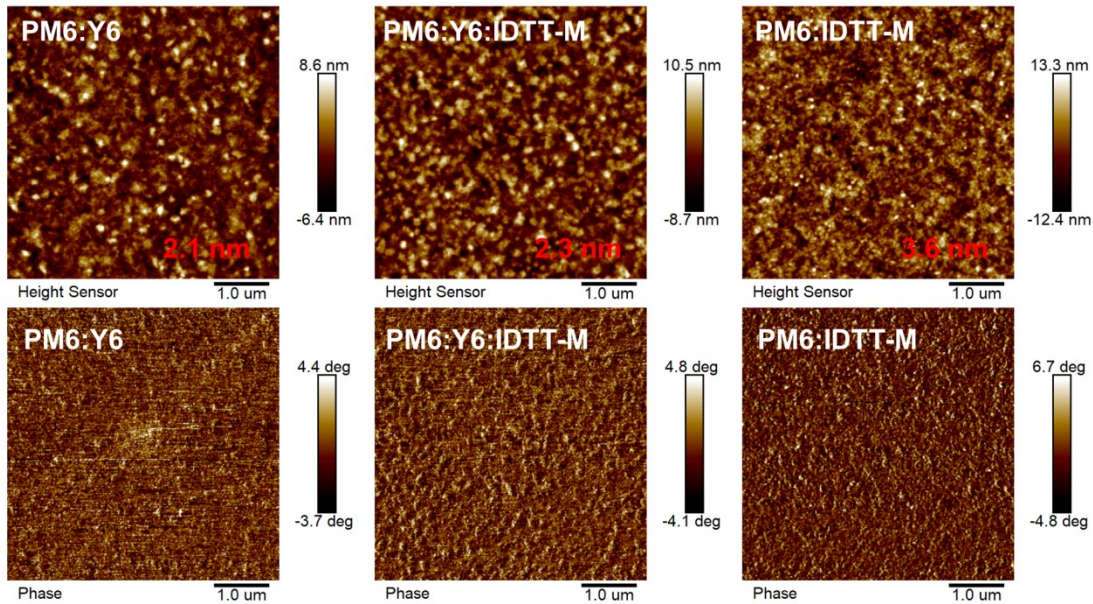


**Figure 4.** AFM height (top) and phase (bottom) images of PM6:Y6, PM6:Y6:IDTT-M (1:1.02:0.18) and PM6:IDTT-M based blend film.

The film morphologies of binary and optimal ternary blend films are investigated by atomic force microscopy (AFM). As shown by the height images in **Figure 4**, PM6:IDTT-M blend films possess a coarse surface with root mean square (RMS) surface roughness of 3.6 nm, while PM6:Y6 and PM6:Y6:IDTT-M (1:1.02:0.18) based blend films show a smoother surface with RMS roughness of approximately 2 nm. Similar to our previous studies, the coarser surface is attributable to the strong crystalline property of IDTT-M. The phase images of PM6:Y6:IDTT-M exhibit obvious fiber-like structures, which are conducive for efficient charge separation and transportation. Grazing incidence wide-angle X-ray scattering (GIWAXS) studies provided further details of molecular packing and crystallization property. The 2D GIWAXS patterns of neat PM6, Y6 and IDTT-M (**Figure S9**), and corresponding line-cuts were shown in **Figure S10** and **Figure S11**. The electron donor PM6 exhibits  $\pi$ - $\pi$  stacking peaks at  $1.68 \text{ \AA}^{-1}$  in both out-of-plane (OOP) direction and in-plane (IP) direction, indicating the coexistence of face-on and edge-on orientations. In contrast, both Y6 and

IDTT-M adopt a preferential face-on orientation, which is evident from a strong IP (100) lamellar stacking peak and the OOP (010)  $\pi$ - $\pi$  stacking peak at  $1.75 \text{ \AA}^{-1}$  and  $1.58 \text{ \AA}^{-1}$ , respectively. In particular, IDTT-M is more crystalline than Y6, as evidenced by the shorter lamellar stacking distance (1.90 nm VS 2.24 nm), narrower full width at the half maximum with larger crystal coherence length and high-order lamellar stacking reflections ( $h00$ ) ( $h = 1, 2, 3$ ) peaks at 0.33, 0.67 and  $0.99 \text{ \AA}^{-1}$ , respectively. The 2D GIWAXS patterns of binary and ternary blend films and corresponding line-cuts are shown in **Figure 5**. All the ternary blend films and PM6:Y6 based blend film adopt a preferred face-on orientation. This is evident from the disappearance of diffraction (100) peaks at  $0.31 \text{ \AA}^{-1}$  (**Figure S10**) and the remarkable (010) diffraction peaks at  $1.75 \text{ \AA}^{-1}$  (**Figure S11**) in the OOP direction. When the third component of IDTT-M in ternary blend films is not more than 20 wt%, the (100) diffraction peaks at IP direction and (010) diffraction peaks at OOP direction remain unchanged, implying that molecular packing is dictated by Y6, and IDTT-M is combined into the framework of Y6 without altering the molecular packing pattern or staying in the amorphous region to form a mixture at the molecular scale (alloy-like structure). Interestingly, an obvious shoulder peak at  $0.33 \text{ \AA}^{-1}$  (**Figure 5c**) appears and the (010) peak shifts from  $1.75 \text{ \AA}^{-1}$  to  $1.71 \text{ \AA}^{-1}$  (**Figure 5b**) in the ternary blend film with 30 wt% IDTT-M. Such result suggests the formation of segregated crystalline IDTT-M domains that also impacts the packing of the PM6 domain in the blend film. This trend is consistent with the high crystallinity of IDTT-M, which doesn't mix well with the PM6 domain — in the binary blend film based on PM6:IDTT-M, there are characteristic but distinctive sets of (100) and (010) diffraction peaks from both PM6 and IDTT-M. The poor phase separation behavior due to the high crystallinity of IDTT-M leads to lower device performance. As a result, after incorporating 30 wt% IDTT-M in the ternary blend films,  $J_{SC}$  and FF of ternary device (1:0.84:0.36) decrease noticeably from  $25.81 \text{ mA cm}^{-2}$  to  $23.68 \text{ mA cm}^{-2}$ , and from 73.89% to 68.00%, respectively. These

morphological studies indicate that at optimized blend ratio, the high crystallinity of IDTT-M can be mitigated and forms intermixed phases within the Y6 domain, which also helps to orient PM6 to the favorable face-on packing that is advantageous for vertical charge transport and improved hole mobility.

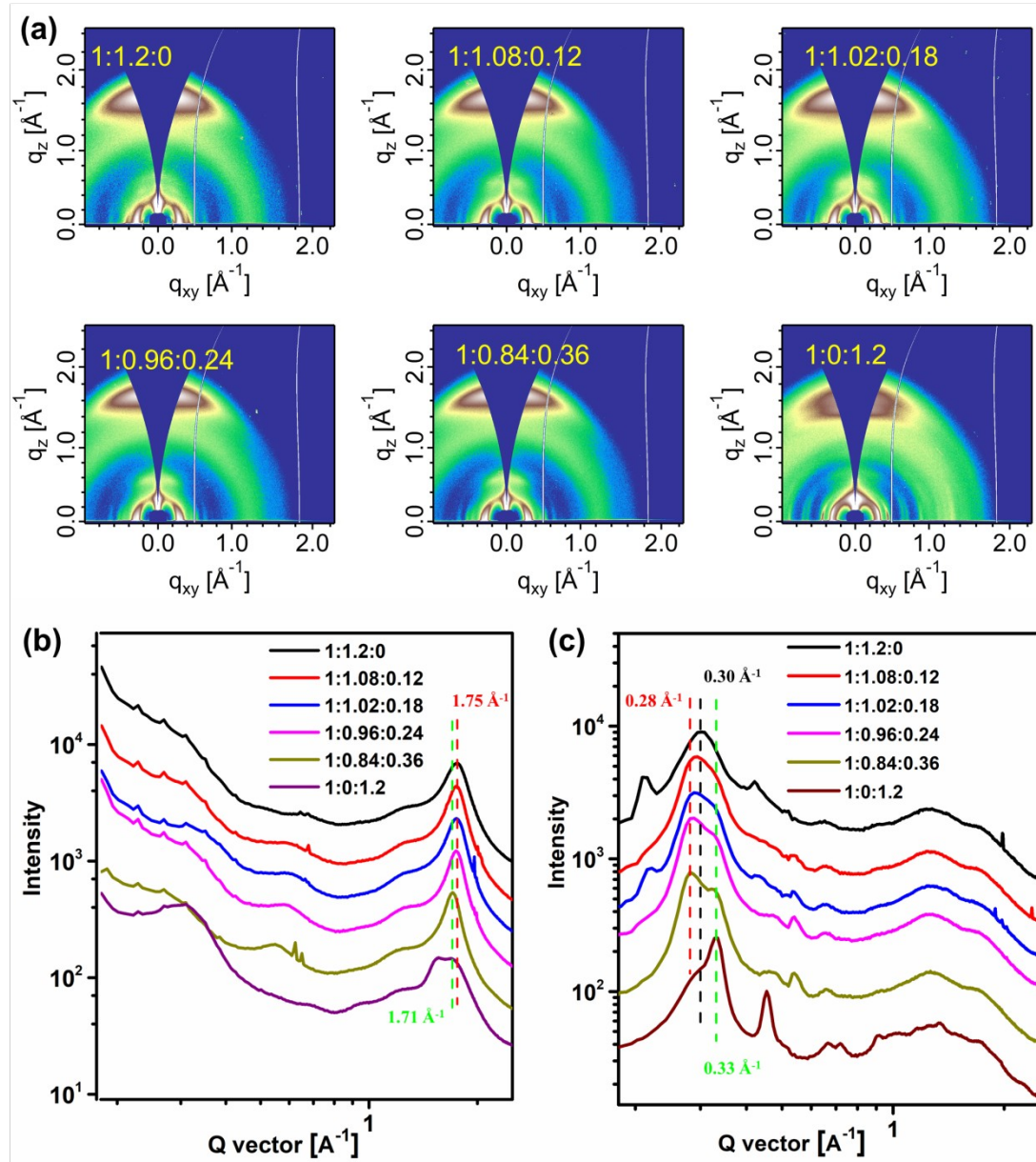


**Figure 5.** (a) 2D GIWAXS patterns; (b) GIWAXS line-cuts in the out-of-plane direction and (c) in the in-plane direction of binary and ternary blend films with different weight ratios of IDTT-M.

### 3. Conclusion

A highly crystalline and wide bandgap electron acceptor, IDTT-M was used to fabricate high efficiency ternary solar cells with PM6 and another narrow bandgap electron acceptor Y6. When compared to its binary counterparts, the optimized ternary solar cells (PM6:Y6:IDTT-M=1:1.02:0.18) deliver the best PCE as high as 16.63% with simultaneously enhanced  $J_{SC}$  from 25.41 mA cm<sup>-2</sup> to 25.81 mA cm<sup>-2</sup>,  $V_{OC}$  from 0.841 V to 0.872 V, and FF from 72.45% to 73.89%. Although incorporation of IDTT-M in the ternary systems leads to decreased absorption in the long wavelength region, benefiting from efficient FRET between IDTT-M and Y6, EQE values are enhanced not only in the short wavelength region but also in the long wavelength region, leading to an elevated  $J_{SC}$ . At the same time, it also provides an efficient non-radiative pathway to facilitate exciton dissociation and more efficient channels that results in improved hole transfer. Morphological studies further reveal that the proper mixture of the two acceptors helps to induce PM6 to form face-on orientation with non-disrupted PM6:Y6 bi-continuous nanophase separations, which are responsible for improved carrier mobility and suppressed recombination. Furthermore, the  $V_{OC}$  of the ternary devices is monotonically elevated due to the higher LUMO energy levels of IDTT-M. Our results demonstrate that a ternary blend with efficient FRET is a promising strategy to further advance the organic photovoltaic technology to a higher standard even without fully complementary absorption.

### Supporting Information

Supporting Information is available from the Wiley Online Library or from the author.

### Acknowledgements

L. X. was supported by the financial support from the National Natural Science Foundation of China (51903057) and we also thank the support from the National Key

Research and Development Program of China (2020YFB0408100) and Guangdong Innovative and Entrepreneurial Research Team Program (2016ZT06C412). Part of this work was performed as a user project at the Molecular Foundry, and the GIWAXS data was collected at beamline 7.3.3 at the Advanced Light Source (ALS) at Lawrence Berkeley National Laboratory, both supported by the Office of Science, Office of Basic Energy Sciences, of the US Department of Energy under contract No. DE-AC02-05CH11231.

Received: ((will be filled in by the editorial staff))

Revised: ((will be filled in by the editorial staff))

Published online: ((will be filled in by the editorial staff))

## References

- [1] a) S. Berny, N. Blouin, A. Distler, H.-J. Egelhaaf, M. Krompiec, A. Lohr, O. R. Lozman, G. E. Morse, L. Nanson, A. Pron, T. Sauermann, N. Seidler, S. Tierney, P. Tiwana, M. Wagner, H. Wilson, *Adv. Sci.* **2016**, 3, 1500342; b) G. Zeng, J. W. Zhang, X. B. Chen, H. W. Gu, Y. W. Li, Y. F. Li, *Sci. China Chem.* **2019**, 62, 851.
- [2] a) Y. Liu, J. Zhao, Z. Li, C. Mu, W. Ma, H. Hu, K. Jiang, H. Lin, H. Ade, H. Yan, *Nat. Commun.* **2014**, 5, 5293; b) Z. C. He, B. Xiao, F. Liu, H. B. Wu, Y. L. Yang, S. Xiao, C. Wang, T. P. Russell, Y. Cao, *Nat. Photonics* **2015**, 9, 174; c) J. H. Wan, X. P. Xu, G. J. Zhang, Y. Li, K. Feng, Q. Peng, *Energy Environ. Sci.* **2017**, 10, 1739; d) B. Kan, M. M. Li, Q. Zhang, F. Liu, X. J. Wan, Y. C. Wang, W. Ni, G. K. Long, X. Yang, H. R. Feng, Y. Zuo, M. T. Zhang, F. Huang, Y. Cao, T. P. Russell, Y. S. Chen, *J. Am. Chem. Soc.* **2015**, 137, 3886; e) L. G. Xiao, T. Q. Lai, X. Liu, F. Liu, T. P. Russell, Y. Liu, F. Huang, X. B. Peng, Y. Cao, *J. Mater. Chem. A.* **2018**, 6, 18469; f) D. Deng, Y. Zhang, J. Zhang, Z. Wang, L. Zhu, J. Fang, B. Xia, Z. Wang, K. Lu, W. Ma, Z. Wei, *Nat. Commun.* **2016**, 7, 13740.
- [3] a) T. Ameri, N. Li, C. J. Brabec, *Energy Environ. Sci.* **2013**, 6, 2390; b) Q. S. An, F. J. Zhang, J. Zhang, W. H. Tang, Z. B. Deng, B. Hu, *Energy Environ. Sci.* **2016**, 9, 281.
- [4] a) R. Ma, Y. Tao, Y. Chen, T. Liu, Z. Luo, Y. Guo, Y. Xiao, J. Fang, G. Zhang, X. Li, X. Guo, Y. Yi, M. Zhang, X. Lu, Y. Li, H. Yan, *Sci. China Chem.* **2021**, 64, 581; b) H. Li, Z. Xiao, L. M. Ding, J. Z. Wang, *Sci. Bull.* **2018**, 63, 340; c) L. G. Xiao, B. He, Q. Hu, L. Maserati, Y. Zhao, B. Yang, M. A. Kolaczkowski, C. L. Anderson, N. J. Borys, L. M. Klivansky, T. L. Chen, A. M. Schwartzberg, T. P. Russell, Y. Cao, X. B. Peng, Y. Liu, *Joule* **2018**, 2, 2154; d) H. B. Naveed, W. Ma, *Joule* **2018**, 2, 621; e) Z. Li, C. Yan, L. Xiao, H. Mao, J. Liu, W. Tan, Y. Min, *Org. Electron.* **2021**, 93, 106135; f) Q. S. An, J. Wang, W. Gao, X. L. Ma, Z. H. Hu, J. H. Gao, C. Y. Xu, M. H. Hao, X. L. Zhang, C. L. Yang, F. J. Zhang, *Sci. Bull.* **2020**, 65, 538; g) K. N. Zhang, J. J. Guo, L. J. Zhang, C. C. Qin, H. Yin, X. Y. Gao, X. T. Hao, *Adv. Funct. Mater.* **2021**, 31; h) M. Jiang, H. Bai, H. Zhi, L. Yan, H. Y. Woo, L. Tong, J. Wang, F. Zhang, Q. An, *Energy Environ. Sci.* **2021**, DOI: 10.1039/D1EE00496D; i) S. X. Li, L. L. Zhan, Y. Z. Jin, G. Q. Zhou, T. K. Lau, R. Qin, M. M. Shi, C. Z. Li, H. M. Zhu, X. H. Lu, F. L. Zhang, H. Z. Chen,

*Adv. Mater.* **2020**, 32, 2001160; j) Y. Chang, T. K. Lau, M. A. Pan, X. H. Lu, H. Yan, C. L. Zhan, *Mater. Horiz.* **2019**, 6, 2094; k) R. J. Ma, T. Liu, Z. H. Luo, K. Gao, K. Chen, G. Y. Zhang, W. Gao, Y. Q. Xiao, T. K. Lau, Q. P. Fan, Y. Z. Chen, L. K. Ma, H. L. Sun, G. L. Cai, T. Yang, X. H. Lu, E. G. Wang, C. L. Yang, A. K. Y. Jen, H. Yan, *ACS Energy Lett.* **2020**, 5, 2711; l) J. L. Song, C. Li, L. Zhu, J. Guo, J. Q. Xu, X. N. Zhang, K. K. Weng, K. N. Zhang, J. Min, X. T. Hao, Y. Zhang, F. Liu, Y. M. Sun, *Adv. Mater.* **2019**, 31, 1905645; m) S. He, Z. C. Shen, J. D. Yu, H. L. Guan, G. H. Lu, T. Xiao, S. T. Yang, Y. P. Zou, L. J. Bu, *Adv. Mater. Interfaces* **2020**, 7, 2000577; n) T. T. Yan, W. Song, J. M. Huang, R. X. Peng, L. K. Huang, Z. Y. Ge, *Adv. Mater.* **2019**, 31, 1902210.

- [5] a) L. Hong, H. Yao, Z. Wu, Y. Cui, T. Zhang, Y. Xu, R. Yu, Q. Liao, B. Gao, K. Xian, H. Y. Woo, Z. Ge, J. Hou, *Adv. Mater.* **2019**, 31, 1903441; b) X. P. Xu, K. Feng, Z. Z. Bi, W. Ma, G. J. Zhang, Q. Peng, *Adv. Mater.* **2019**, 31, 1901872; c) R. J. Ma, T. Liu, Z. H. Luo, Q. Guo, Y. Q. Xiao, Y. Z. Chen, X. J. Li, S. W. Luo, X. H. Lu, M. J. Zhang, Y. F. Li, H. Yan, *Sci. China Chem.* **2020**, 63, 325; d) Y. Cui, H. F. Yao, J. Q. Zhang, K. H. Xian, T. Zhang, L. Hong, Y. M. Wang, Y. Xu, K. Q. Ma, C. B. An, C. He, Z. X. Wei, F. Gao, J. H. Hou, *Adv. Mater.* **2020**, 32, 1908205; e) J. Wu, G. Li, J. Fang, X. Guo, L. Zhu, B. Guo, Y. Wang, G. Zhang, L. Arunagiri, F. Liu, *Nat. Commun.* **2020**, 11, 1; f) Q. S. Liu, Y. F. Jiang, K. Jin, J. Q. Qin, J. G. Xu, W. T. Li, J. Xiong, J. F. Liu, Z. Xiao, K. Sun, S. F. Yang, X. T. Zhang, L. M. Ding, *Sci. Bull.* **2020**, 65, 272; g) X. Guo, Q. Fan, J. Wu, G. Li, Z. Peng, W. Su, J. Lin, L. Hou, Y. Qin, H. Ade, *Angew. Chem. Int. Ed.* **2021**, 60, 2322; h) S. X. Li, C. Z. Li, M. M. Shi, H. Z. Chen, *ACS Energy Lett.* **2020**, 5, 1554; i) L. L. Ye, Y. H. Cai, C. Li, L. Zhu, J. Q. Xu, K. K. Weng, K. N. Zhang, M. F. Huang, M. Zeng, T. F. Li, E. J. Zhou, S. T. Tan, X. T. Hao, Y. P. Yi, F. Liu, Z. H. Wang, X. W. Zhan, Y. M. Sun, *Energy Environ. Sci.* **2020**, 13, 5117; j) M. Zhang, L. Zhu, G. Zhou, T. Hao, C. Qiu, Z. Zhao, Q. Hu, B. W. Larson, H. Zhu, Z. Ma, Z. Tang, W. Feng, Y. Zhang, T. P. Russell, F. Liu, *Nat. Commun.* **2021**, 12, 309; k) C. Li, J. Zhou, J. Song, J. Xu, H. Zhang, X. Zhang, J. Guo, L. Zhu, D. Wei, G. Han, J. Min, Y. Zhang, Z. Xie, Y. Yi, H. Yan, F. Gao, F. Liu, Y. Sun, *Nat. Energy* **2021**, DOI: 10.1038/s41560-021-00820-x; l) Y. Cui, H. Yao, J. Zhang, T. Zhang, Y. Wang, L. Hong, K. Xian, B. Xu, S. Zhang, J. Peng, Z. Wei, F. Gao, J. Hou, *Nat. Commun.* **2019**, 10, 2515; m) L. Liu, Y. Kan, K. Gao, J. Wang, M. Zhao, H. Chen, C. Zhao, T. Jiu, A.-K.-Y. Jen, Y. Li, *Adv. Mater.* **2020**, 32, 1907604; n) Q. Guo, Q. Guo, Y. F. Geng, A. L. Tang, M. J. Zhang, M. Z. Du, X. N. Sun, E. J. Zhou, *Mater. Chem. Front.* **2021**, 5, 3257.
- [6] a) Y. Z. Lin, J. Y. Wang, Z. G. Zhang, H. T. Bai, Y. F. Li, D. B. Zhu, X. W. Zhan, *Adv. Mater.* **2015**, 27, 1170; b) J. Yuan, Y. Q. Zhang, L. Y. Zhou, G. C. Zhang, H. L. Yip, T. K. Lau, X. H. Lu, C. Zhu, H. J. Peng, P. A. Johnson, M. Leclerc, Y. Cao, J. Ulanski, Y. F. Li, Y. P. Zou, *Joule* **2019**, 3, 1140.
- [7] Y. Wu, Y. Zheng, H. Yang, C. K. Sun, Y. Y. Dong, C. H. Cui, H. Yan, Y. F. Li, *Sci. China Chem.* **2020**, 63, 265.
- [8] K. Jiang, Q. Y. Wei, J. Y. L. Lai, Z. X. Peng, H. Kim, J. Yuan, L. Ye, H. Ade, Y. P. Zou, H. Yan, *Joule* **2019**, 3, 3020.
- [9] a) N. An, Y. Cai, H. Wu, A. Tang, K. Zhang, X. Hao, Z. Ma, Q. Guo, H. S. Ryu, H. Y. Woo, Y. Sun, E. Zhou, *Adv. Mater.* **2020**, 32, 2002122; b) A. Tang, W. Song, B. Xiao, J. Guo, J. Min, Z. Ge, J. Zhang, Z. Wei, E. Zhou, *Chem. Mater.* **2019**, 31, 3941; c) B. He, B. Yang, M. A. Kolaczkowski, C. A. Anderson, L.

- M. Klivansky, T. L. Chen, M. A. Brady, Y. Liu, *ACS Energy Lett.* **2018**, 3, 1028; d) X. Li, G. Huang, N. Zheng, Y. Li, X. Kang, S. Qiao, H. Jiang, W. Chen, R. Yang, *Sol. RRL* **2019**, 3, 1900005; e) X. Liu, X. Du, J. Wang, C. Duan, X. Tang, T. Heumueller, G. Liu, Y. Li, Z. Wang, J. Wang, F. Liu, N. Li, C. J. Brabec, F. Huang, Y. Cao, *Adv. Energy Mater.* **2018**, 8, 1801699.
- [10] a) W. Ni, M. M. Li, B. Kan, F. Liu, X. J. Wan, Q. Zhang, H. T. Zhang, T. P. Russell, Y. S. Chen, *Chem. Commun.* **2016**, 52, 465; b) Y. Gong, Z. Kan, W. Xu, Y. Wang, S. H. AlShammary, F. Laquai, W.-Y. Lai, W. Huang, *Sol. RRL* **2018**, 2, 1800120.
- [11] a) L. Lu, W. Chen, T. Xu, L. Yu, *Nat. Commun.* **2015**, 6, 7327; b) L. Yang, W. Gu, L. Hong, Y. Mi, F. Liu, M. Liu, Y. Yang, B. Sharma, X. Liu, H. Huang, *ACS Appl. Mater. Interfaces* **2017**, 9, 26928; c) J. Gao, R. Ming, Q. An, X. Ma, M. Zhang, J. Miao, J. Wang, C. Yang, F. Zhang, *Nano Energy* **2019**, 63, 103888.
- [12] L. Xiao, M. A. Kolaczkowski, Y. Min, Y. Liu, *ACS Appl. Mater. Interfaces* **2020**, 12, 41852.
- [13] a) N. K. Elumalai, A. Uddin, *Energy Environ. Sci.* **2016**, 9, 391; b) R. A. Street, D. Davies, P. P. Khlyabich, B. Burkhardt, B. C. Thompson, *J. Am. Chem. Soc.* **2013**, 135, 986.
- [14] a) W. Y. Su, Q. P. Fan, X. Guo, X. Y. Meng, Z. Z. Bi, W. Ma, M. J. Zhang, Y. F. Li, *Nano Energy* **2017**, 38, 510; b) Y. Chen, P. Ye, Z.-G. Zhu, X. Wang, L. Yang, X. Xu, X. Wu, T. Dong, H. Zhang, J. Hou, F. Liu, H. Huang, *Adv. Mater.* **2017**, 29, 1603154.
- [15] Y. L. Ma, D. D. Cai, S. Wan, P. S. Wang, J. Y. Wang, Q. D. Zheng, *Angew. Chem. Int. Ed.* **2020**, 59, 21627.
- [16] L. Xiao, C. Yan, Z. Li, W. Zhong, W. Tan, Y. Liu, F. Liu, X. Peng, Y. Min, *ACS Appl. Energy Mater.* **2021**, 4, 4234.
- [17] D. Li, L. Zhu, X. Liu, W. Xiao, J. Yang, R. Ma, L. Ding, F. Liu, C. Duan, M. Fahlman, Q. Bao, *Adv. Mater.* **2020**, 32, 2002344.
- [18] a) L. Yang, W. X. Gu, L. Hong, Y. Mi, F. Liu, M. Liu, Y. F. Yang, B. Sharma, X. F. Liu, H. Huang, *ACS Appl. Mater. Interfaces* **2017**, 9, 26928; b) J. S. Huang, T. Goh, X. K. Li, M. Y. Sfeir, E. A. Bielinski, S. Tomasulo, M. L. Lee, N. Hazari, A. D. Taylor, *Nat. Photonics* **2013**, 7, 480; c) V. Gupta, V. Bharti, M. Kumar, S. Chand, A. J. Heeger, *Adv. Mater.* **2015**, 27, 4398; d) N. Gasparini, S. Kahmann, M. Salvador, J. D. Perea, A. Sperlich, A. Baumann, N. Li, S. Rechberger, E. Spiecker, V. Dyakonov, G. Portale, M. A. Loi, C. J. Brabec, T. Ameri, *Adv. Energy Mater.* **2019**, 9, 1803394.

A highly crystalline and wide bandgap electron acceptor, IDTT-M is used to fabricate high efficiency ternary solar cells with PM6 and another narrow bandgap electron acceptor Y6. benefiting from efficient FRET and the formed molecular mixture of the two acceptors, a significantly improved PCE up to 16.63% is achieved with simultaneously enhanced  $J_{SC}$ ,  $V_{OC}$  and FF.

*Liangang Xiao<sup>a</sup>, Xing Wu<sup>a</sup>, Guoxing Ren<sup>a</sup>, Matthew A. Kolaczkowski<sup>b</sup>, Guang Huang<sup>d</sup>, Wanyi Tan<sup>a</sup>, Lin Ma<sup>d</sup>, Yidong Liu<sup>a</sup>, Xiaobin Peng<sup>c</sup>, Yonggang Min<sup>\*a</sup> and Yi Liu<sup>\*b</sup>*

**Highly Efficient Ternary solar cells with efficient Förster resonance energy transfer for simultaneously enhanced photovoltaic parameters**

ToC figure ((Please choose one size: 55 mm broad × 50 mm high **or** 110 mm broad × 20 mm high. Please do not use any other dimensions))

